Retinal Vascular Tree Morphology: A Semi-automatic Quantification.

M. Elena Martínez-Pérez [a*], Alun D. Hughes [b], Alice V. Stanton [b], Simon A. Thom [b], Neil Chapman [b], Anil A. Bharath [a] and Kim H. Parker [a]

Abstract— **A semi-automatic method to measure and quantify geometrical and topological properties of continuous vascular trees in clinical fundus images is described. Measurements are made from binary images obtained with a previously described segmentation process. The skeletons of the segmented trees are produced by thinning, branch and crossing points are identified and segments of the trees are labelled and stored as a chain code. The operator selects a tree to be measured and decides if it is an arterial or venous tree. An automatic process then measures the lengths, areas and angles of the individual segments of the tree. Geometrical data and the connectivity information between branches from continuous retinal vessel trees are tabulated. A number of geometrical properties and topological indices are derived. Vessel diameters and branching angles are validated against manual measurements and several derived geometrical and topological properties are extracted from red-free fundus images of 10 normotensive and 10 age and sex matched hypertensive subjects and compare with previously reported results.**

Keywords— **retinal imaging, vascular geometry, vascular topology, image analysis, ophthalmology, vacular tree morphology.**

I. Introduction

Retinal blood vessel morphology can be an important indicator for diseases such as diabetes, hypertension and arteriosclerosis. Both the arteries and veins of the retina are generally binary trees, whose properties can be considered either locally or globally. Measurable geometrical changes in diameter, branching angle, length or tortuosity, as a result of disease, have been described in retinal blood vessels [1], [2], [3]. The detection and measurement of retinal blood vessels can be used to quantify the severity of disease, as part of the process of automated diagnosis of disease or in the assessment of the progression of therapy. Thus a reliable method of vessel detection and quantification would be valuable.

The analysis of geometry and network properties of branching structures is not new. Branching structures are common in nature, occurring in such diverse phenomena as river networks, lightning discharge pathways, erosion channels in porous media and airways of the lung and as well as blood vessels. Biological branching trees have been studied with many different imaging and image processing techniques. However, retinal blood vessel tree geometry and topology have not been widely studied by means of image processing.

Quantitative analysis of retinal blood vessels from fundus images have usually been studied in terms of individual bifurcations, measuring a few of the most clearly visible bifurcations in an image. Most of these studies have focused mainly on diameter measurements [4], [5] although others also included midline detection [6], [7] and tortuosity measurements [6], [8]. Those studies that have characterised continuous blood vessel trees from retinal images, by means of image processing techniques, have been mainly focused on the detection process rather than the measurement of geometrical or topological properties [9], [10], [11].

In this paper a semi-automatic method to measure and tabulate geometrical data as well as connectivity information from continuous retinal vessel trees is presented. Data are extracted from binary images obtained from a previously developed segmentation method [12]. The procedure consists of a semi-automatic labelling of the skeleton trees followed by an automatic procedure for measurement and generation of tabulated data for further analysis. Several geometrical and topological indices are extracted. The methods are validated by comparison with manual measurements and applied to a pilot study of 10 normal and 10 hypertensive subjects and differences between groups in the morphological properties are investigated.

II. Vessel segmentation

Blood vessels are segmented using a previously described algorithm based on multi-scale analysis [12]. Two geometrical features based upon the first and the second derivative of the intensity image, maximum gradient and principal curvature, are obtained at different scales by means of Gaussian derivative operators. A multiple pass region growing procedure is used which progressively segments the blood vessels using the feature information together with spatial information about the 8-neighbouring pixels. The algorithm works with red-free as well as fluorescein retinal images. Fig. 1(a) shows the scanned negative of a red-free retinal photograph and (b) the segmented binary image where the optic disc region is manually marked in grey, vessels are tracked from this area outwards.

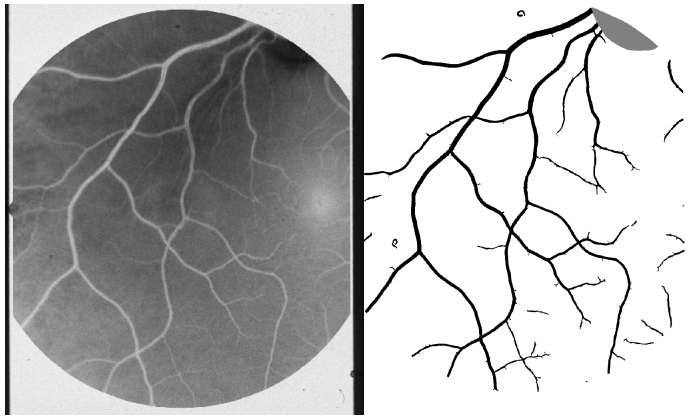

(a) (b)

Fig. 1. (a) Scanned negative of a red-free fundus image (size 1168×1021 pixels), (b) the segmented binary image with the optic disc manually marked in grey, vessel trees are tracked from this area outwards.

III. Tree Labelling

A. Thinning

The skeleton of the vascular tree is obtained from the segmented binary image by a thinning process where pixels are eliminated from the boundaries towards the centre without destroying connectivity in an 8-connected scheme [13]. A pruning process is applied to eliminate short, false spurs, due to small undulations in the vessel boundary. False spurs are deleted if they are smaller or equal to the largest vessel diameter expected in a particular image. Fig. 2(a) shows a cropped image from a negative fluorescein angiograph, (b) shows the segmented tree in grey and the skeleton of the tree in black.

[a] Department of Bioengineering. Imperial College of Science, Technology and Medicine. Prince Consort Road, London, SW7 2BY, UK.

[b] Clinical Pharmacology, National Heart and Lung Institute, Imperial College of Science, Technology and Medicine, St Mary's Hospital, South Wharf Road, London, W2 1NY, UK.

Martínez-Pérez would like to acknowledge to the Mexican National Council for Science and Technology (CONACYT) for financial support.

* Contact to: Elena.Martinez@enst.fr

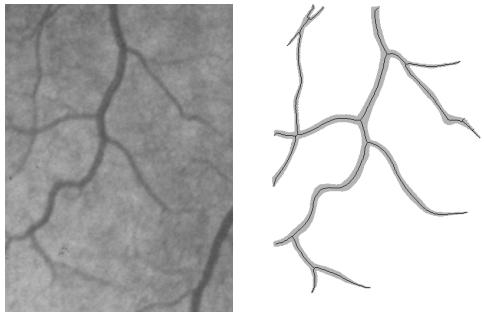

(a) (b)

Fig. 2. Thinning process: (a) cropped image of a scanned negative fluorescein angiograph, (b) segmented tree in grey and the skeleton of the tree marked in black.

B. Detecting significant points

Three types of significant points in the skeleton must be detected: terminal points, bifurcation points and crossing points. In a first pass, skeleton pixels with only one neighbour in a 3×3 neighbourhood are labelled as terminal points and pixels with 3 neighbours are labelled as candidate bifurcation points. Because vessel crossing points appear in the skeleton as two bifurcation points very close to each other, a second pass is made using a fixed size circular window centered on the candidate bifurcations, the window diameter is set equal to the largest vessel diameter expected in that particular image. Fig. 3(a) shows the candidate points marked with circles over the skeleton and (b) summarises the three possible cases; where two intersections with the window are spurs, three intersections are bifurcation points and four intersections are crossing points. Once all of the significant points are identified, bifurcation points are labelled as -r, where r is the radius of the maximum circle centered on that point that fits inside the boundary of the bifurcation (Fig. 3(c) and 5(a)). The sign is used to distinguish between the radius and chain code numbers that are described in the following section. For crossing points the skeleton is corrected and marked to define a single crossing point (see the last row of Fig. 3(b)). Fig. 3(c) shows the corrected skeleton with all of the significant points marked.

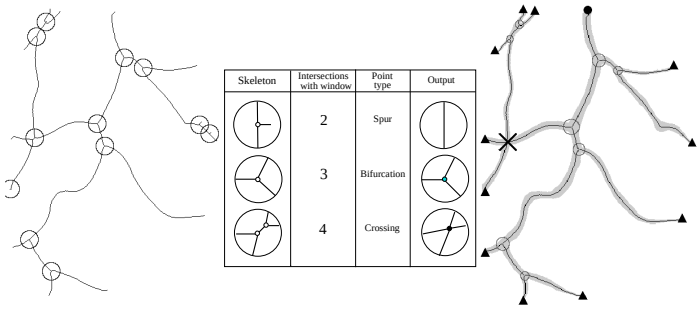

(a) (b) (c)

Fig. 3. Detecting significant points: (a) candidate points marked with circles over the skeleton, (b) types of significant points and (c) corrected skeleton with significant points marked: bifurcations points are marked with the maximum circle that fits inside the vessel boundaries, terminal points with triangles, crossing points with crosses and the root point with a black circle.

Until this stage the process is fully automatic. The process fails when a) two true bifurcation points are very close and are merged into a crossing point or b) when two vessels cross at a very acute angle so that the two candidate bifurcation points fall outside the circular window and are thus defined as two bifurcation points. An example is shown in the top-left corner in Fig. 3(c) where two branching points are found, an inspection of the full image shows that it should be a crossing point. These cases must be corrected manually. The complete image is labelled in this way and it normally contains several independent vascular trees.

C. Tracking

Each tree is tracked individually. Fig. 4(a) shows an example of an idealised skeleton denoted as 1's, where the root and terminal points are marked with -1 and the bifurcation point with $-r$.

For the tracking process, the user points to the root segment of the tree to be tracked and the algorithm searches for its unique terminal point (-1). The coordinates of this point are saved and a chain code is automatically generated starting at this point, specifying the direction of the next skeleton point as shown in Fig. 4(b), Fig. 4(d) shows the chain code directions in a 3×3 neighbourhood. When the first bifurcation point is reached the chain of the current branch is ended and the coordinates of the starting points of the two daughters are found and saved. The process is repeated iteratively for every branch of the tree until a terminal point is reached and all daughters have been numbered with the chain code (Fig. 4(c)). In order to keep the network information about the relationships between branches along the tree, a binary ordering scheme is adopted by labelling the root as 1 and thereafter the daughters of parent k_0 are labelled with *key* numbers $k_1 = 2k_0$ and $k_2 = 2k_0 + 1$. Fig. 4(e) shows the numbering scheme used. With this numbering scheme we are able to track the tree in either direction.

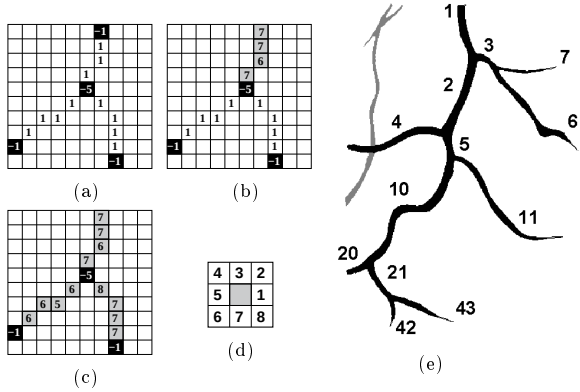

(a) (b) (c) (d) (e)

Fig. 4. Tracking. (a) Root and terminal points from the skeleton are marked with -1 and the bifurcation points with $-r$ before tracking, (b) interim step of the tracking where a chain code is generated from the root outwards, specifying the direction of the next skeleton point, (c) the process is iteratively repeated for every branch of the tree until a terminal point is reached and all daughters have been numbered and (d) the chain code directions in a 3×3 neighbourhood. (e) The root is labelled 1 and thereafter the daughters of parent k_0 are labelled $k_1 = 2k_0$ and $k_2 = 2k_0 + 1$.

IV. Measurement of Tree Geometrical Properties

A. Lengths

Two lengths are measured directly from the skeleton. The true length of the branch from the starting to the end point of the skeleton computed as $L_t = N_o + \sqrt{2}N_e$ where N_o and N_e are the number of pixels with odd and even direction codes along the skeleton, and the Euclidean end-to-end distance L_s (or straight length Fig. 5(c)).

B. Areas

Using the value of the radius defined at each bifurcation point, a circle and a line tangent to this circle and perpendicular to the skeleton are drawn on the border image at each end of the branch. This is done to close the region to be measured as illustrated in Fig. 5(a) and to ensure that ambiguities in the area near bifurcation points are excluded. The number of vessel pixels bounded by these tangents is defined as the area A. The average diameter of the selected branch is calculated as $d = A/L_a$, where L_a is the true length of the segment measured along the skeleton between the bounding lines (Fig. 5(a)). When two blood vessels cross, the borders in the crossing region for both vessels are opened (Fig. 5(b)). These borders are closed by taking a section of the skeleton centered at the crossing point and displacing it parallel to the skeleton in both directions until maximum correlations of pixels with the border are found (Fig. 5(c)). This maintains the natural shape of the curvature of the vessel in the crossing region.

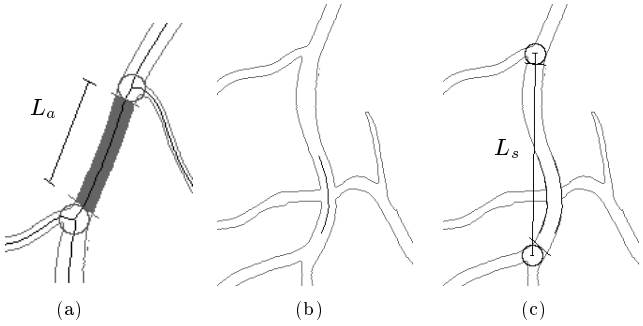

Fig. 5. Areas. (a) The area A is the number of vessel pixels bounded by the two lines tangent to the circles and perpendicular to the skeleton, and L_a is the true length of the section of the skeleton. In (b) and (c) the borders at crossing points are closed using displaced sections of the skeleton.

C. Angles

A bifurcation angle is associated with each parent vessel. Because a vessel can be very tortuous, and because daughters can be parents themselves, three different angles are measured for each individual segment: the *total* angle of the branch, a *head* angle and a *tail* angle (Fig. 6(a)). The total angle of the branch is computed along the total true length of the skeleton line, the head and tail angles are calculated over a distance of 5 times the radius of the particular bifurcation point along the true length of the section of the skeleton used for the angle calculation (Fig. 6(b)).

Each angle j (for $j = 0 \ldots 2$) is measured as a length-averaged angle defined as $\psi_j = \frac{1}{L}\sum_{i=1}^{N} w_i \gamma_i$, where γ_i is the associated angle of the skeleton pixel i (45° steps in a 3×3 neighbourhood), w_i is the associated weight in the chain code $w_i = 1$ when i is odd and $w_i = \sqrt{2}$ when i is even, N is the number of pixels in the section of the skeleton and L is the true length of the section of the skeleton (Fig. 6(c)).

V. Organisation of the tabulated data

One data table per tree is generated during the measurement process. Each row represents an individual segment which contains 10 columns: i) key number, ii) true and straight lengths: L_t, L_s in pixels, iii) area and the length at which this area was computed: A, L_a in pixels, iv) total, head and tail angles: γ_{total}, γ_{head}, γ_{tail} in degrees, and v) key numbers of the two daughters: k_1, k_2, which for terminal segments are empty. The user identifies each tree as arterial or venous.

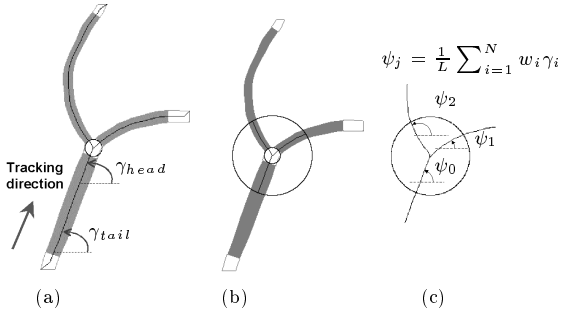

Fig. 6. Angles. (a) Three angles are measured per segment: *total*, *head* and *tail*, (b) *head* and *tail* angles are defined and measured over a distance of 5 times the radius defined in the bifurcation point, and (c) average angles ψ_j are computed as shown.

These are the basic geometrical measurements needed to derive other geometrical descriptors for individual bifurcations. Using the key numbers, the data can be indexed to track daughter and/or parent geometrical properties along the complete tree and study the connectivity within the tree. It also allows topological properties of the trees to be quantified.

VI. Derived morphological properties

A. Geometrical properties

A number of non-dimensional parameters that are independent of the scale of the image can be derived from the basic measurements.

Expansion factor: sum of the cross sectional areas of the two daughter branches divided by the area of the parent $\alpha = (d_1^2 + d_2^2)/d_0^2$, where indices 0, 1, 2, denote the parent vessel, the major and minor daughter vessels, respectively.
Asymmetry factor: the cross sectional area of the minor daughter divided by that of the major $\beta = d_2^2/d_1^2$. With $0 < \beta \leq 1$, being equal to one for a symmetrical bifurcation.
Junction exponent: the exponent x relating the parent and daughter vessel diameters $d_0^x = d_1^x + d_2^x$. Murray suggested that $x = 3$ in arteries optimised for minimum work [14]. Although this equation is highly non-linear, both sides are monotonic in x and the solution is easily found by an iterative search procedure.
Branching angle: $\omega = \theta_1 + \theta_2$.
Angle of daughters: angles of each daughter with respect to the parent $\theta_1 = \psi_1 - \psi_0$ and $\theta_2 = \psi_2 - \psi_0$ (see Fig. 6(c)).
Angular asymmetry: the difference between branching angles of the minor and the major daughters $\phi = \theta_2 - \theta_1$.
Length to diameter ratio: $\lambda = L_t/d$.
Tortuosity: $T = L_t/L_s$. With $1 < T \leq \infty$, being equal to one for a straight segment.

Properties d, L_t, λ and T describe individual segments whereas α, β, ω, θ_1, θ_2 and ϕ are bifurcation descriptors.

B. Topological properties

Since we have information about the connectivity between branches, we can also make topological analyses of the vascular trees. A vascular tree is generally a binary rooted tree; a tree in which one vertex is designated as the root and there are at most three edges (or segments) contiguous with any vertex [15].

Some important topological features of biological trees are those that describe how much a branching structure deviates from a symmetrical tree. The topological indices most commonly used in biological applications are [16]. 1) The Strahler

branching ratio, R_m, is calculated by ordering all the edges within a given tree using Strahler ordering. This ordering scheme assigns all external edges an order of one. Where two edges of order m come together, the third edge is assigned to order $m+1$. Where an edge of order m meets an edge of order n, the third edge is assigned to order $max(m,n)$. R_m is defined as $R_m = \frac{N_m}{N_{m+1}}$ where N_m is the number of edges of order m. Fig. 7(a) shows Strahler ordering scheme from the same tree shown in Fig. 4(e). The significance of R_m is that it indicates a degree of topological self-similarity in the branching structure. 2) The altitude, A_l, is defined as the largest external path length, where an external path length is defined as the number of edges between the root and the terminal edge. 3) The total path length, P_e, is the sum of all the external path lengths. Fig. 7(b) shows an example where $A_l = 6$ and $P_e = 30$. 4) The number of external-internal edges, N_{E_I}, where an E_I edge is an edge which is terminal and its sister is non-terminal. In Fig. 7(c) $N_{E_I} = 3$ and the total number of terminal edges is $N_T = 7$. The number of external-external edges $N_{E_E} = N_T - N_{E_I}$. Finally, 5) the tree asymmetry index, $A_s = \frac{N+1-2A_l}{2^{A_l}-2A_l}$ where $N = N_T * 2 - 1$ is the total number of edges. Its value ranges from zero to one for a symmetrical tree.

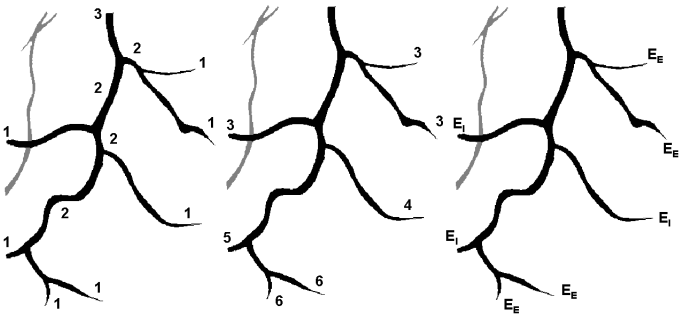

(a) (b) (c)

Fig. 7. Topological indices: (a) Strahler ordering scheme where the branching ratio is: $R = N_m/N_{m+1}$, (b) Altitude ($A_l = 6$) and total path length ($P_e = 30$), and (c) number of external-internal edges ($N_{E_I} = 3$), where the total number of terminal edges is $N_T = 7$.

VII. Validation studies

Since direct *in vivo* measurements of retinal blood vessels in humans are not feasible, two indirect validation studies were undertaken: a comparison of our measurements with manual measurements of diameters and branching angles of individual bifurcations, and a pilot study of the changes in the geometrical properties in arterial trees in untreated hypertensive patients in comparison with those reported in the literature.

A. Comparison with manual measurements

Automatic measurements of individual bifurcations were compared with manual measurements for 17 randomly chosen bifurcations from red-free retinal subimages taken by an expert from images of 2400 × 2800 pixels. The manual measurements involved the average of 5 diameters measured close to the bifurcation and the angles between straight lines fitted by eye. Since each bifurcation involves 3 vessels, 17 bifurcation angles, ω, and 51 diameter vessels, d, were measured.

In the absence of a true measure, we defined a normalised difference between measures X_A and X_M as:

$$\Delta X = \frac{X_A - X_M}{< X >}, \quad \text{where} \quad < X >= \frac{1}{2}(X_A + X_M) \qquad (1)$$

X_A corresponds to automatic measurements and X_M to manual [17]. Table I summarises the results.

TABLE I

Automatic against manual measurement comparisons for red-free individual bifurcations. d diameter and ω branching angle. The differences $X_A - X_M$, where subscripts refer to automatic (A) and manual (M), are expressed in pixels for d and degrees for ω. The p values are calculated using the two sided Wilcoxon signed-rank test.

Feature	$X_A - X_M$	ΔX	n	p
d	-2.40 ± 2.65	-0.14 ± 0.16	51	≤ 0.001
ω	7.34 ± 8.03	0.12 ± 0.11	17	≤ 0.006

For d, automatic were smaller than manually measured diameters, whereas for ω automatic were larger than manual angles. These differences can not be taken as error but only as indication of the variation between different measurement techniques.

B. A pilot study of the effect of hypertension

The geometrical and topological properties were measured in red-free fundus images (583 × 509 pixels) from 10 normotensive and 10 hypertensive subjects. Both groups consisted of 6 females and 4 males and were age matched: normal, median age 46 years, range 33-55; hypertensive, median age 43.5, range 34-52. Hypertension was diagnosed on the basis of 3 or more successive sitting blood pressures $140/90 mmHg$ or above: normal, mean $121.7/72.5 mmHg$, range 134/79 - $114/83 mmHg$; hypertensive, mean $159.5/97 mmHg$, range 194/120 - $141/96 mmHg$. The hypertensive subjects were all untreated prior to retinal photography.

Table II summarises the median and quartiles of the derived geometrical properties used for the comparison. p values were calculated using the Wilcoxon rank test for all features and * denotes a significant difference between groups ($p < 0.05$). d, L_t, d_0, d_1 and d_2 are in pixels; ω in degrees. In d all diameters d_0, d_1 and d_2 are consider together. A pixel corresponds to approximately 15 μm based on the diameter of the optic disc ($1.5\ mm \approx 98$ pixels) for this scale of images with squared pixels (no geometrical correction of the spherical field of view was considered).

TABLE II

Median and quartiles values of the derived geometrical properties measured in arterial trees, of normotensive, N, and hypertensive, H, groups. n = number of bifurcation or number of segments depending on the geometrical property. In d all vessels are considered (d_0, d_1 and d_2). p values are calculated using the two sided Wilcoxon rank test, * denotes significant difference ($p < 0.05$).

Feature	Group	Median	1^{st} Qu	3^{rd} Qu	n	p
d	N	3.28	2.06	4.84	290	0.185
	H	3.31	2.15	3.99	147	
ω	N	84.50	72.22	98.02	138	0.809
	H	84.75	72.35	97.55	67	
L_t	N	52.51	24.76	92.46	290	< 0.001
	H	78.53	51.14	136.09	147	*
λ	N	14.91	7.34	26.12	290	< 0.001
	H	26.00	14.33	39.19	147	*
d_0	N	4.69	3.49	5.64	138	0.006
	H	4.00	3.47	4.73	67	*
d_1	N	4.34	3.01	5.41	138	0.042
	H	3.76	3.23	4.50	67	*
d_2	N	2.22	1.70	3.25	138	0.505
	H	2.13	1.71	3.03	67	

The length to diameter ratio, λ, is larger for hypertensives (in

agreement with [3]), the total number of blood vessels, n, decreases with hypertension so-called "rarefaction" (in agreement with [1]) and there is a reduction in vessel diameters for d_0 and d_1 for hypertensives ([18] found the same for d). Branching angles have been reported to be more acute in hypertensives in a earlier study [2], but we did not find any significant difference in our data.

The analysis of the topological parameters showed that both arterial and venous trees are asymmetric. The number of terminal edges, N_T, and the total path length normalised by the total number of terminals, P_e/N_T, are significantly different in hypertensive subjects. We are unaware of any previous measurements of these topological properties in retinal vessels that can be used for comparison.

VIII. Conclusions

We have developed a semi-automatic method to measure and quantify the geometrical and topological properties of retinal blood vessels from fundus retinal images. Based on segmented binary images, a semi-automatic labelling of the skeleton trees is described followed by an automatic procedure to measure length, area and angles and the connectivity between branches. The main advantages are the ability to track and measure complete vessel trees almost automatically. This allows us to analyse more images and measure many more properties of the retinal vasculature.

Zhou, *et. al.* [6] developed an algorithm to track the midline and extract diameters and tortuosity of a single vessel segment, although only diameter measurements were reported. Their algorithm needs starting and ending points and a tracking direction defined by an operator. Wu *et. al.* [4] measured the width of segments of retinal arteries and veins but only near the optic disc based on edge detectors and boundary tracing in which the operator marked starting and ending points on the edge of the vessel border to be measured. This procedure is repeated with both vessel borders and the average diameter is calculated.

Our technique needs manual user interaction in the correction of the significant points, and in the identification of the tree to be measured. No tracking direction or ending points are needed since they are implicit in the chain code. The algorithm is able to track a complete segmented vessel tree.

Tolias *et.al.* [7] developed an unsupervised fuzzy algorithm for vessel detection in red-free fundus images based on the tracking algorithm of [6]. The main differences are: the initialisation step is automatic and it tracks the complete trees of the whole retinal image beginning in an area near the optic disc. Their quantitative results for the efficiency of vessel tracking were made on 3 different complete images in which 27, 24 and 17 vessel segments were identified but not measured. Hart *et.at.* [8] presented an automatic technique for measuring blood vessel tortuosity from complete retinal images. From the skeletons of 20 images 981 blood vessel segments were extracted using a linear classifier and their tortuosity was measured. In comparison, we are able to measure 1030 vessel segments from the 20 retinal images used in our pilot study with all of the geometrical descriptors and connectivity information discussed above. Akita *et.al.* [19] did extract network information from retinal subimages but only to help in the detection of the optic disc. Hart *et.at.* [8] also reported a vessel network tortuosity indirectly measured by using a weighted additivity of all the blood vessel segments in an image rather than by direct tracking. As far as we are aware, no previous work has been reported using the topological indices proposed herein for the study of retinal blood vessels.

The purpose of this pilot study is not to reach any conclusions about physiology, but to show the kinds of analyses that could be applied to provide insights about the changes due to diseases such as hypertension in the geometry and topology of the retinal vasculature derived from clinical fundus images. The appearance of the retinal blood vessels can be an important diagnostic indicator of various clinical disorders of the eye and the body as a whole. We have shown that the (nearly) automatic method of morphological quantification proposed in this paper is sensitive enough to show differences in geometrical changes due hypertension already reported in the literature. It also suggests that analysis of the geometry and topology of a continuous vascular network may provide more sensitive indicators of changes due to disease.

References

[1] H.A.J. Struijker, J.L.M. le Noble, M.W.J. Messing, M.S.P. Huijberts, F.A.C. le Noble, and H. van Essen, "The microcirculation and hypertension," *J. Hypertens.*, vol. 10, pp. S147–S156, 1992.

[2] A.V. Stanton, B. Wasan, A. Cerutti, S. Ford, R. Marsh, P.P. Sever, S.A. Thom, and A.D. Hughes, "Vascular network changes in the retina with age and hypertension," *J. Hypertens.*, vol. 13, pp. 1724–1728, 1995.

[3] L.A. King, A.V. Stanton, P.S. Sever, S. Thom, and A.D. Hughes, "Arteriolar length-diameter (l:d) ratio: A geometric parameter of the retinal vasculature diagnostic of hypertension," *J. Hum. Hypertens.*, vol. 10, pp. 417–418, 1996.

[4] D-C. Wu, B. Schwartz, J. Schwoerer, and R. Banwatt, "Retinal blood vessel width measured on color fundus photographs by image analysis," *Acta Ophthalmol. Scand.*, vol. 73, pp. 33–40, 1995.

[5] X. Gao, A. Bharath, A. Stanton, A. Hughes, N. Chapman, and S. Thom, "Quantification and characterisation of arteries in retinal images," *Comp. Meth. Program. Biom.*, vol. 63, pp. 133–146, 2000.

[6] L. Zhou, M.S. Rzeszotarski, L.J. Singerman, and J.M. Chokreff, "The detection and quantification of retinopathy using digital angiograms," *IEEE Trans. Med. Imag.*, vol. 13, pp. 619–626, 1994.

[7] Y.A. Tolias and S.M. Panas, "A fuzzy vessel tracking algorithm for retinal images based on fuzzy clustering," *IEEE Trans. Med. Imag.*, vol. 17, pp. 263–273, April 1998.

[8] W.E. Hart, M. Goldbaum, B. Côté, P. Kube, and M.R. Nelson, "Measurement and classification of retinal vascular tortuosity," *Int. J. Med. Inform.*, vol. 53, pp. 239–252, 1999.

[9] S. Chaudhuri, S. Chatterjee, N Katz, M. Nelson, and M. Goldbaum, "Detection of blood vessels in retinal images using two-dimensional matched filters," *IEEE Trans. Med. Imag.*, vol. 8, pp. 263–269, 1989.

[10] F. Zana and J.C. Klein, "Segmentation of vessel-like patterns using mathematical morphology and curvature evaluation," *IEEE Trans. Med. Imag.*, vol. 10, pp. 1010–1019, July 2001.

[11] A. Hoover, V. Kouznetsova, and M. Goldbaum, "Locating blood vessels in retinal images by piecewise threshold probing of a matched filter response.," *IEEE Trans. Med. Imag.*, vol. 19, pp. 203–210, 2000.

[12] M.E. Martínez-Pérez, A.D. Hughes, A.V. Stanton, S.A. Thom, A.A. Bharath, and K.H. Parker, "Retinal blood vessel segmentation by means of scale-space analysis and region growing," in *MICCAI-99*, C. Taylor and A. Colchester, Eds. 1999, vol. 1679 of *Lectures Notes in Computer Science*, pp. 90–97, Springer-Verlag.

[13] W.K. Pratt, *Digital Image Processing*, John Wiley & Sons, Inc., New York, second edition, 1991.

[14] C.D. Murray, "The physiological principle of minimum work. i. the vascular system and the cost of blood volume," *Proc. Nat. Acad. Sci.*, vol. 12, pp. 207–214, 1926.

[15] N. MacDonald, *Trees and Networks in Biological Models*, John Wiley & Sons, New York, 1983.

[16] G.M. Berntson, "The characterization of topology: a comparison of four topological indices for rooted binary trees," *J. Theor. Biol.*, vol. 177, pp. 271–281, 1995.

[17] J. M. Bland and D. G. Altman, "Statistical methods for assessing agreement between two methods of clinical measurement.," *Lancet*, vol. 1, pp. 307–310, February 1986.

[18] A.V. Stanton, P. Mullaney, F. Mee, E.T. O'Brien, and K. O'Malley, "A method of quantifying retinal microvascular alterations associated with blood pressure and age.," *J. Hypertens.*, vol. 13, pp. 41–48, 1995.

[19] K. Akita and H. Kuga, "A computer method of understanding ocular fundus images," *Pattern Recogn.*, vol. 15, pp. 431–443, 1982.